Micro-Inverter Based On Symmetrical Boost-Discharge Topology For Photovoltaic Energy Source

Mohammed El Bachir GHRIBI[1] , *Zine Eddine Touhami TERNIFI*[2] , *Ghalem BACHIR*[2] , *Michel AILLERIE*[3]

[1] Applied Power Electronics Laboratory (LEPA), University of science and technology of Oran Mohamed Boudiaf, Oran, Algeria.
[2] Laboratory of sustainable development of the electrical energy (LDDEE), University of science and technology of Oran Mohamed Boudiaf, Oran, Algeria.
[3] Laboratoire Matériaux Optiques, Photonique et Systèmes (LMOPS), Université de Lorraine, CentraleSupélec,F-57000 Metz, France.

mohammedelbachir.ghribi@univ-usto.dz, touhamyz@yahoo.fr, ghalem.bachir@univ-usto.dz, michel.aillerie@univ-lorraine.fr

Abstract. *This paper demonstrates the performance of a new innovative photovoltaic microinverter topology with high power quality and efficiency. This inverter is based on coupling a boost converter with a discharge circuit to provide a rectified sine wave voltage. In the first part of this paper, we describe the proposed topology and its operating principle as well as the simple and robust control system used. We also verify the stability of the system using the Lyapunov method. In the second part, we present the simulation results and discuss the influence of the load nature on the total harmonic distortion (THD) and on the efficiency.*

Keywords

Photovoltaic micro-inverter, boost, discharge circuit , Lyapunov, total harmonic distortion.

1. Introduction

Researchers are currently dedicating a great deal of efforts to improve photovoltaic inverters and their architectures. Over the past decades, researchers have devoted a lot of effort to improving photovoltaic inverters and their architecture. Their main work has been focused on increasing conversion efficiency, reliability, achieving better grid integration and optimizing the installation of control circuits. Moreover, due to the development of the renewable energy resources, modern grids include microgrids based on distributed energy resources such as photovoltaic arrays or wind turbines and energy storage devices such as batteries and supercapacitors. In this distributed architecture, each resource is connected to the network via its own converter as in the case of photovoltaics (PV) where each panel transmits its energy via a micro-inverter. These last are specially designed to be individually and directly interface between a PV panel and the grid. Thus, when considering PV resource, these micro-inverters appear as many times as there are panels in the PV plant. For this reason and in view of the large number that can be quickly reached, their technology must be as simple as possible while ensuring high conversion efficiency and reliability and their individual cost must be kept as low as possible while guaranteeing a good wave quality of the output voltage and current.

In multilevel inverters the number of switches is proportional to the number of stages. On the other hand, using less stages implies a deterioration of the THD or the obligation of adding filters in the inverter topology [1],[2],[3] and [4]. In order to maintain a good power quality in converter with only one conversion stage and without addition of complexe filters, converter having an input boost DC/DC stage before the

inverter one are preferred [5] and [6]. To elevate the voltage between the PV panel and the grid, boost converters are currently used in various photovoltaic microinverter topologies. Driving by specific algorithms based on optimisation methods (we can site the perturb and observe method, fuzzy logic method and the ones using a neural network approaches) boost converter allows following the maximum power point and pre-regulates the voltage and current waveform [7],[8] and [9]. When combining the converter with a discharge circuit and an innovative control, it can provide a high quality sinusoidal voltage, which can be amplified by means of a step-up transformer.

In the current contribution, to reduce the conversion losses and finally the manufacturing costs, the proposed topology does not use a filter. It integrates two converters that operates symmetrically composed by a DC/DC boost with high frequency switches followed by a discharge stage. The topology imposes two conditions on the control. The first one is the consideration in the control of the absolute error's value and the second one is to continue to assume the maintain of a good dynamic response. These two conditions degrade the performance of conventional controllers and those operating in sliding mode. For this reason, in order to obtain better dynamics, we have chosen an exponential action control for the microinverter.

This work presents the performances of this symmetrical boost-discharge microinverter (SBD-converter) topology and its control. In PV source, not only the energy available at the input link to irradiance and temperature of the PV panel influe the quality and quantity of the photovoltaic resource. Indeed, the nature of the load, resistive, capacitive, its size and dynamic, also have a huge influence on the stability and on the functioning of the converters. Thus, in this contribution, we also study the robustness of the proposed microinverter to variations of the load nature.

2. Symmetrical boost-discharge converter topology

The SBD-converter incorporates two circuits in a cascade, as shown in Fig. 1. The first one is a boost converter which allows to charge the capacitor and consequently increase the DC input voltage. The second circuit is composed of a switch in series with a discharge inductance. Its role is discharging the boost capacitor which causes a voltage drop. The inductance increases the discharge time, and thus by translation decreases the average switching frequency that must also be sufficiently low to allow a zero crossing. A resistor can be added in series to limit the current but will have, as consequence an increase of the losses in the conver-
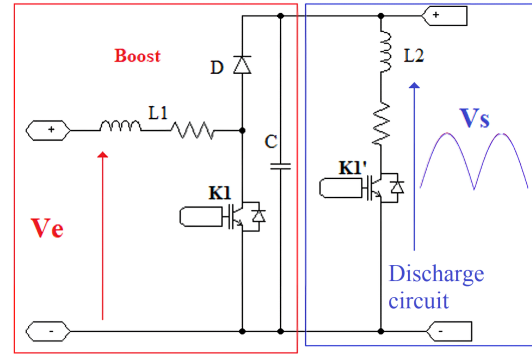

Fig. 1: Schematic diagram of the SBD-converter.

sion process. A diode is inserted between the boost switch K1 and the capacitor to force it to discharge via the load and the discharge circuit. The symmetrical operation of the two switches, K1 and K1', enables the voltage to track the reference waveform. It has the same waveform as the voltage an uncontrolled full-wave rectifier of, a rectified sine wave.

The rectified sine voltage at the boost output is converterdto a 50 Hz sine wave using a simple 180° command. [11] and [12]. The maximum voltage output is set to twice the input which is supplied by a 44 V panel in no-load condition ($V_{ref} = |88.sin(2\pi 50t)|$). A transformer is added to reach a 220 V output in-order to feed a standard load.

2.1. Symmetrical boost-discharge converter modeling

To model the SBD-converter, the power switches states (K1 and K1') are denoted using a Boolean variable (S), S also represents the control signal status of the two switches, zero for off and one for on. A resistor represents the load. As shown in Fig. 2, the operating modes include two phases corresponding to the states of the switches, when both are open or closed.

Phase 1. The power switches are blocked.
The energy produced by the photovoltaic source is stored in the capacitor C, the voltage increases. The equations describing this phase are as follows:

$$\frac{dI_{L1}}{dt} = -\frac{V_s}{L1} + \frac{V_e}{L1} \tag{1}$$

$$\frac{dI_{L2}}{dt} = 0 \tag{2}$$

$$\frac{dV_s}{dt} = \frac{I_{L1}}{C} - \frac{V_s}{RC} \tag{3}$$

Phase 2. The power switches are on.
Due to the diode isolating the first stage, the capacitor

discharges in the second stage. The equations describing this phase are as follows:

$$\frac{dI_{L1}}{dt} = \frac{V_e}{L1} \tag{4}$$

$$\frac{dI_{L2}}{dt} = \frac{V_s}{L_2} \tag{5}$$

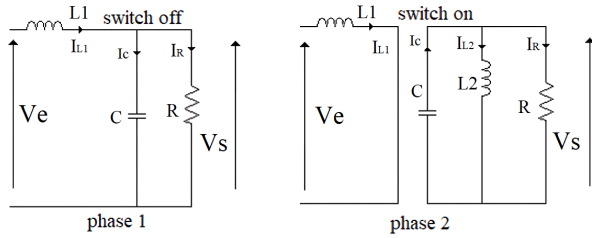$$\frac{dV_s}{dt} = \frac{-I_{L2}}{C} + \frac{-V_s}{RC} \tag{6}$$

Fig. 2: Equivalent circuit of the Boost and discharge circuit with the switches on and off.

Matrix representation of both functioning phases.

It is convenient for the analysis of these two phases of the operating mode to expressed them by a matrix. From eq (1-6) the state representation of the system is as follow:

$$\begin{bmatrix} \frac{dI_{L1}}{dt} \\ \frac{dI_{L2}}{dt} \\ \frac{dV_s}{dt} \end{bmatrix} = \begin{bmatrix} 0 & 0 & \frac{S-1}{L1} \\ 0 & 0 & \frac{S}{L2} \\ \frac{1-S}{C} & \frac{-S}{C} & \frac{-1}{RC} \end{bmatrix} \begin{bmatrix} I_{L1} \\ I_{L2} \\ V_s \end{bmatrix} + \begin{bmatrix} \frac{1}{L1} \\ 0 \\ 0 \end{bmatrix} .V_e$$

$$\tag{7}$$

2.2. Sizing of the various electronic components

The boost inductance value can be obtained by the expression of the current oscillations ΔI_{L1} [13]. Both expressions are given by equation 8, We have considered a microinverter dedicated to a PV panel constituted of 60 silicon cells in series. Thus, the panel voltage at maximum power is 36 V. It is noted V_{e-max}.

$$\Delta I_{L1} = \frac{\alpha.T.V_{e-max}}{L1} \Rightarrow L_1 \approx \frac{V_{e-max}(1 - \frac{V_{e-max}}{V_{s-max}})}{4.\Delta I_{L1}.f_s} \tag{8}$$

The switching frequency is variable because it is related to the energy produced by the PV source depending on the irradiation and temperature of the PV panel, and the energy transmitted to the load. This switching frequency is delivered by the tracker to follow the

reference voltage. The frequency is limited between 2 kHz and 20 kHz to limit the discharge current. The discharge inductance is calculated from the minimum frequency and the maximum current through it. The resistance in series with the discharge inductance is neglected, as shown in equation 10.

$$L_2 \frac{dI_{L2}}{dt} + (R_{L2} + R_{K1'}).I_{L2} = V_s(t) \tag{9}$$

$$\frac{dI_{L2}}{dt} = \frac{V_s}{L_2} \rightarrow I_{L2} = \frac{V_s}{L_2}.t \tag{10}$$

$$\begin{aligned} L_{2-min} &= \frac{\epsilon_p}{I_{L2-max} \cdot f_{com-min}} \\ L_{2-max} &= \frac{V_{s-max}}{I_{L2-max} \cdot f_{com-min}} \end{aligned} \tag{11}$$

The maximum boost capacity needs to supply the average boost current, and discharges completely in a quarter of a period yielding to the following equation 12:

$$\begin{aligned} I_c &\approx \frac{2.I_{s-max}}{\pi} \\ C_{max} &= \frac{I_c.\Delta t}{\Delta V} = \frac{I_c}{4.f_s.\Delta V} \approx \frac{I_{s-max}}{2.\pi.f_s.V_{s-max}} \end{aligned} \tag{12}$$

In this equation, I_{s-max} represents the maximum current supplied by the inverter. Tests show that the ideal capacity is $\frac{2}{5}C_{max}$.

2.3. Symmetrical boost-discharge converter control

The principle of the control used is based on the minimisation of the distance between the desired convergence point and the actual operating point. It consists in minimising the error between the desired and the real operation. In the following we will call this distance "ε" corresponding to the error to be minimised in the convergence process.

$$\varepsilon = V_{ref} - V_s \tag{13}$$

The boost command must prevent switch K1 from staying open when ε is negative. If the switch stays open, the output voltage becomes constant and equal to the input voltage. The command uses the absolute value of the error. It introduces, then, an exponential action to speed up the dynamic of the control process. The control signal that imposes the state of the switches (K1 and K1') is given by the following function:

$$S = step(e^{k.|\varepsilon|} - k_1) \tag{14}$$

k and k_1 are two positive constants. The absolute error's value imposes that the output voltage to always be greater or equal to the reference voltage, as shown

in the Fig. 3. This permanent static error is proportional to the natural logarithm of K1, and is calculated as follows:

$$|\varepsilon_p| = \frac{ln(k_1)}{k} \qquad (15)$$

The output voltage is always higher than the reference and is noted:

$$V_s = \sqrt{\varepsilon_p^2 + \frac{4.\varepsilon_p.V_{Rm}}{\pi} + \frac{V_{Rm}^2}{2}} \qquad (16)$$

The maximum reference voltage of the boost, V_{Rm} is calculated according to the desired output voltage yielding to the following equation

$$V_{Rm} = \sqrt{2}V_s - \frac{4}{\pi}\varepsilon_p \qquad (17)$$

In practice, this formula is valid if the capacity is correctly dimensioned ($C \approx \frac{2}{5}C_{max}$). If the capacitor is undersized, the voltage oscillations will be greater, the RMS voltage will be higher than the expected voltage (16), in case of oversizing, the zero crossing will no longer be guaranteed. The error is chosen to be greater than or equal to the voltage drops created by the diode of the boost and the switches of the inverter bridge.
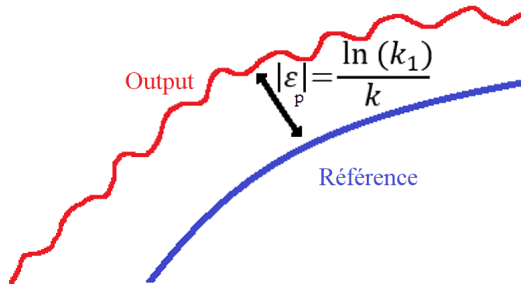

Fig. 3: Static error of the exponential action.

2.4. Symmetrical boost-discharge converter control stability by Lyupanov Method

The stability study of the proposed control is carried out using the Lyapunov method. This method is effective for studying the global or partial stability of a dynamic system. Lyapunov uses an energy function, usually a quadratic function, to determine the stability of an equilibrium point or a motion, this method is applied in this case for a non-linear system that switches between two states. For a system to be stable, the Lyapunov function must be null at the origin, it is defined so that it is always strictly positive and its derivative must be strictly negative,[14],[15]and[16]. The command imposes two switching lines to $V_{ref} + \frac{ln(k_1)}{k}$, and $V_{ref} - \frac{ln(k_1)}{k}$ and the study of the stability allows to

say if the switching lines are attractive or repulsive (as shown in Fig. 4).

The chosen Lyapunov function is given by equation 18. In order to simplify the calculations and to respect the first condition $V(0) = 0$, the variable used for Lyapunov function cancels itself out when K1 and $K'1$ are switched, it is proportional to the error on the voltage, and is given by equation 19.

$$V(\varepsilon_1) = \frac{\varepsilon_1^2}{2} \qquad (18)$$

$$\varepsilon_1 = |\varepsilon| - \frac{ln(k_1)}{k} \qquad (19)$$

$$\varepsilon < 0 \to \varepsilon_1 = -\varepsilon - \frac{ln(k_1)}{k} \to \varepsilon_1' = V_s';$$
$$\varepsilon > 0 \to \varepsilon_1 = \varepsilon - \frac{ln(k_1)}{k} \to \varepsilon_1' = -V_s' \qquad (20)$$

Phase 1: The switches K1 and K1' will be blocked

$$-\frac{ln(k_1)}{k} < \varepsilon < 0 \to -\frac{ln(k_1)}{k} < \varepsilon_1 < 0 \to S = 0 \qquad (21)$$

When the switches K1 and K1' are blocked, the capacitor charges from the source, the voltage across the capacitor increases, which increases the error until a permanent value. Kirchhoff's voltage law proves that.

$$I_{L1} > \frac{V_s}{R} \qquad (22)$$

This means that equation 3 shows that:

$$V_s' > 0 \to \varepsilon_1' > 0 \qquad (23)$$

Phase 2: The switches will be turned on

$$\varepsilon < -\frac{ln(k_1)}{k} \to \varepsilon_1 > 0 \to S = 1 \qquad (24)$$

When the switches are turned on, the capacitor is discharged either through the discharge circuit or the load. The voltage at the terminals of the capacitor decreases and tends towards the reference, which leads the decreasing of the error. This phase, as described by the Equation 6, yields that Vs and I$_{L2}$ are positive. Thus, we can write :

$$V_s' < 0 \to \varepsilon_1' < 0 \qquad (25)$$

The Lyapunov function is strictly positive and for both cases its derivative is strictly negative.

$$V(0) = 0; \ V(\varepsilon_1) = \frac{\varepsilon_1^2}{2}; \ V(\varepsilon_1)' = \varepsilon_1'.\varepsilon_1 \qquad (26)$$

Equations 27 and 28 show that when the voltage is lower than the reference voltage the system becomes

unstable.

$$0 < \varepsilon < \frac{ln(k_1)}{k} \;\rightarrow\; -\frac{ln(k_1)}{k} < \varepsilon_1 < 0 \;\rightarrow\; S = 0$$
$$\rightarrow\; V_s' > 0 \;\rightarrow\; \varepsilon_1' < 0 \;\rightarrow\; V(\varepsilon_1)' > 0 \tag{27}$$

$$\frac{ln(k_1)}{k} < \varepsilon \;\rightarrow\; \varepsilon_1 > 0 \;\rightarrow\; S = 1$$
$$\rightarrow\; V_s' < 0 \;\rightarrow\; \varepsilon_1' > 0 \;\rightarrow\; V(\varepsilon_1)' > 0 \tag{28}$$

The system is stable when the voltage converges to $V_{ref} + \frac{ln(k_1)}{k}$, and unstable when it diverges to $V_{ref} - \frac{ln(k_1)}{k}$. Thus, if the boost voltage falls below the reference voltage minus the permanent error, switches K1 and K1' remain open for the rest of the half period, the source and load are short-circuited. To avoid this problem in operation, the switching frequency must be sufficiently high in relation to the time response of the converter. Fig. 4 clearly illustrates the different zones where the different operating points of the converter are located.
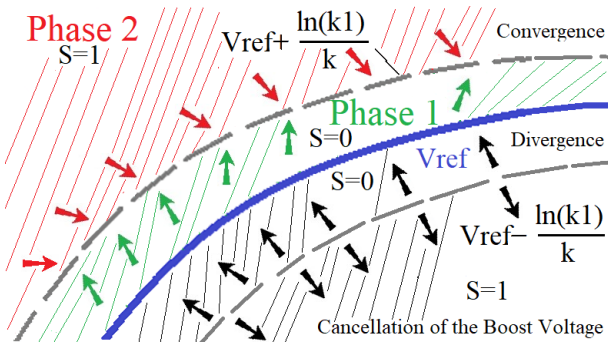

Fig. 4: Lyapunov stability.

3. Simulation results & discussion

The simulation is carried out using the Power Simulation software (PSIM), which directly integrates the FFT analysis and THD calculation. The employed algorithm is based on the radix-2/decimation-in-frequency methodology.

For the simulation we choose to use a permanent error equal to $\varepsilon_p = \frac{ln(k_1)}{k} = 1$ V, the boost inductance is 180 mH, the capacitance is 100 μF and the discharge inductance is 1.5 mH .

It is to be noted that this analysis point out that without the discharge circuit, the control will not allow a sufficient decrease of the boost voltage. In this case, the voltage wouldn't not pass through zero which would deteriorate the THD and will increase the switching losses. This case is illustrated in Fig. 5.
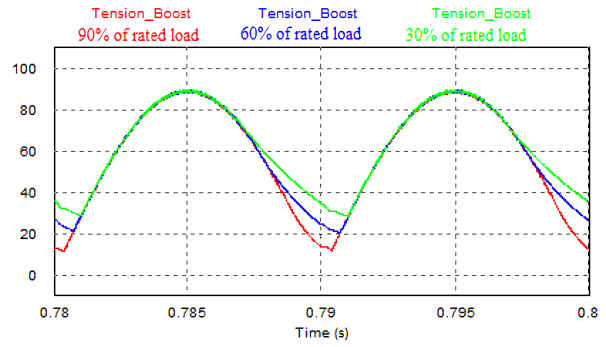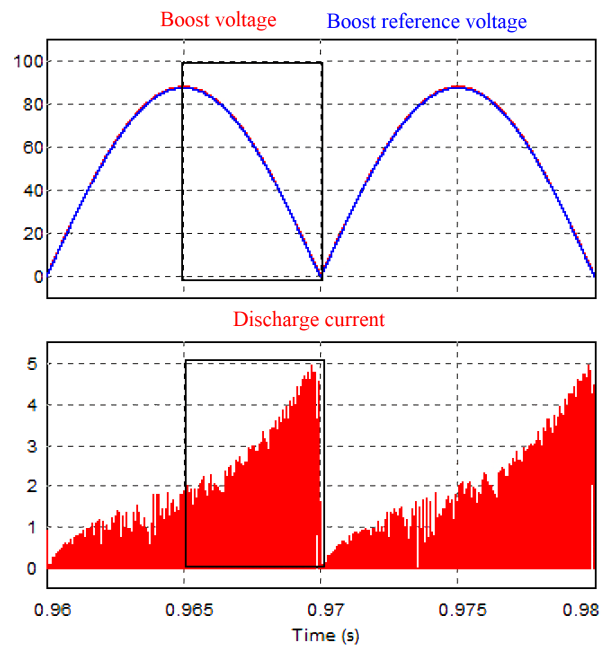

Fig. 5: Voltage of the Boost without the discharge circuit.

.	RMS	Value Average
Boost voltage	62.8 V	56.5
Voltage Boost-Ref	62.22 V	56.03
Discharge current	.	0.5 A

Fig. 6: Voltage of the Boost with the discharge circuit.

The discharge circuit allows a rapid voltage decrease without a perfect zero crossing. When the output voltage of the boost tends to decrease, the supercharging capacitor of the discharge circuit, by discharging, attempts to compensate for this voltage drop. The circuit also avoids voltage instabilities during rise, as shown in Fig. 6.

The power difference between the photovoltaic generator and the load is dissipated by the discharge circuit. The system must initially be sized in a balanced way between the power delivered by the source and that consumed by the load at the risk of having a high total harmonic distortion rate following the conversion. Indeed, too low loads or an oversized photo-

voltaic source lead to excess power loss, increasing the THD compared to that obtained for a nominal load.

The boost output waveform allows 180° control of the inverter bridge switches, the second half-period is inverted, resulting in a sinusoidal voltage of Fig. 7, for this case the load is purely resistive, the THD of the voltage lower than 1.4 %, i.e. at a commonly acceptable level and the output voltage is higher than the reference of 0.6 V.
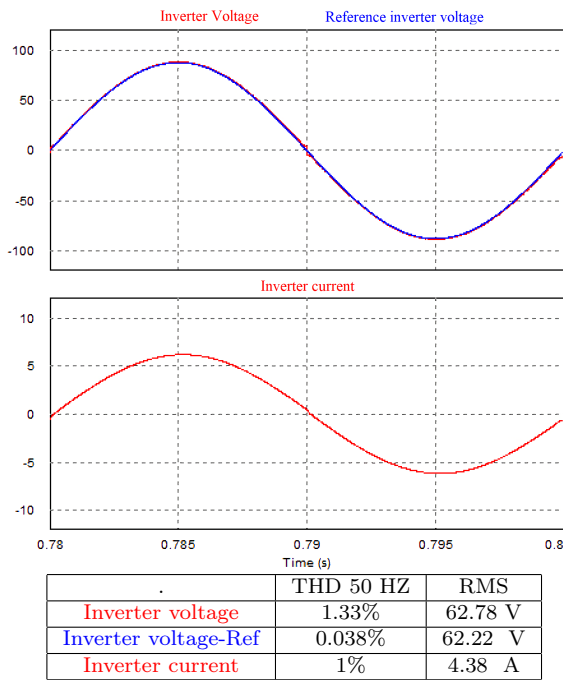

.	THD 50 HZ	RMS
Inverter voltage	1.33%	62.78 V
Inverter voltage-Ref	0.038%	62.22 V
Inverter current	1%	4.38 A

Fig. 7: Inverter output (Current, Voltage) with a purely resistive load.

The control is robust whatever the load as long as it remains below the maximum power of the boost. In the case where the load is purely inductive, the THD remains below the acceptable limits, as shown in the Fig. 8, the voltage THD degrades to 3% for the purely inductive load, the difference between the RMS output voltage and the reference increases to 2 V.

As we can see in previous Figures, we have sized the symmetrical boost-discharge converter an output voltage around 62 V, easily implemented for the experimental part of this work. This voltage is not high enough to feed the grid or a standard load directly. Of course, directly reaching a 220 V of RMS voltage of the grid is achievable with a proper sizing of the boost but, in this topology, it would increase the losses and worsen the harmonic level. The RMS output voltage is much higher than the reference voltage. Fig. 9 show the direct output without transformer. The THD of the voltage is 4.5% with a difference between the efficase voltage of the inverter and the reference of 8 V. The simplest solution to this problem the adding of a
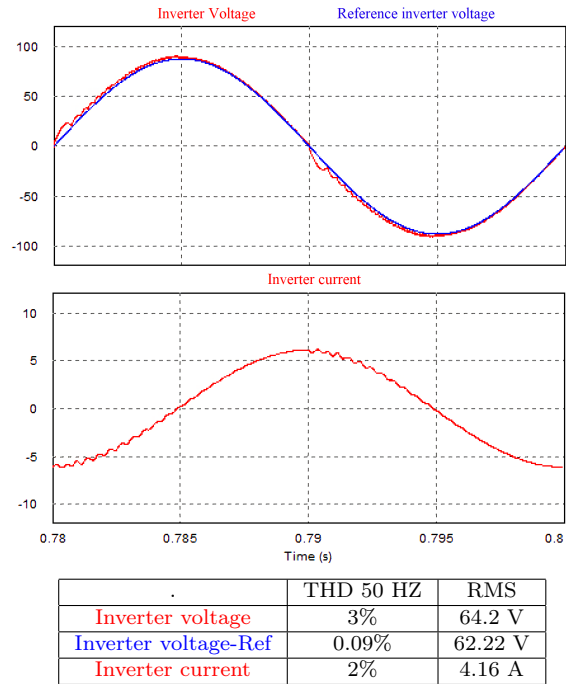

.	THD 50 HZ	RMS
Inverter voltage	3%	64.2 V
Inverter voltage-Ref	0.09%	62.22 V
Inverter current	2%	4.16 A

Fig. 8: Inverter output (Current, Voltage) with a purely inductive load.

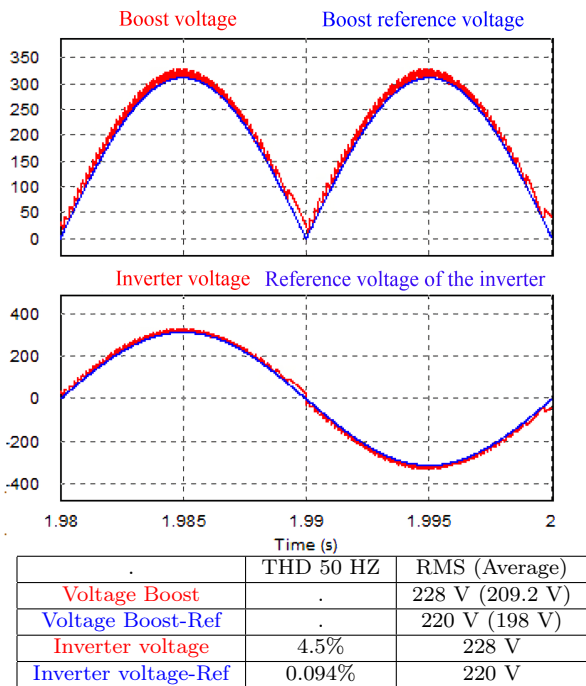| .	THD 50 HZ	RMS (Average)
Voltage Boost	.	228 V (209.2 V)
Voltage Boost-Ref	.	220 V (198 V)
Inverter voltage	4.5%	228 V
Inverter voltage-Ref	0.094%	220 V

Fig. 9: Direct output without transformer.

step-up transformer to reach the desired output voltage. We have implemented this solution and experimental results are shown in Fig. 10. The THD is only 1.08 % for the voltage and current at the transformer output.
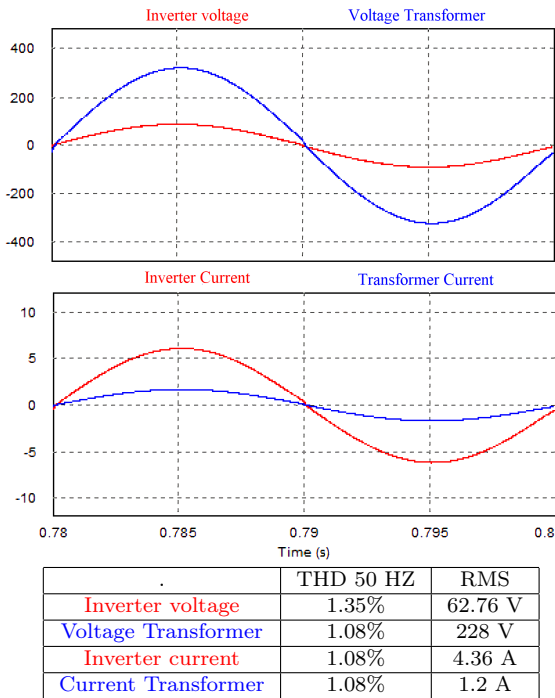
.	THD 50 HZ	RMS
Inverter voltage	1.35%	62.76 V
Voltage Transformer	1.08%	228 V
Inverter current	1.08%	4.36 A
Current Transformer	1.08%	1.2 A

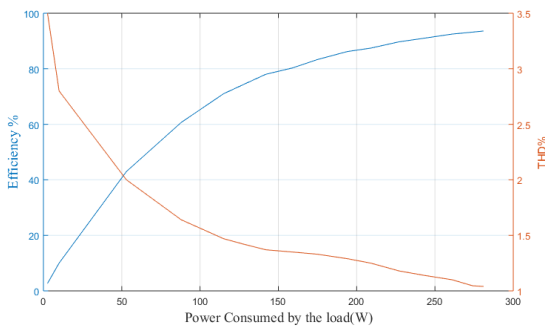**Fig. 10:** Transformer output (Current, Voltage).

Fig. 11: Estimated inverter efficiency. and evolution of THD as a function of load.

For a constant and nominal irradiation and temperature, the current supplied by the panel does not significantly vary. If the consumed power decreases, the surplus power is dissipated in the discharge circuit. The closer the load is to the maximum bearable load the better the efficiency will be, as illustrated in the Fig. 11. The converter's efficiency is promising in nominal operation; the losses increase with the decrease of the load.

In nominal operation, the THD resulting of the output voltage conversion is found very good (around 1 %). As previously mentioned, it deteriorates the more the load decreases. The worst THD is attained in a no-load operation (3.5%), as shown in the Fig. 11 .

Using proteus, the simulation results show an average switching frequency between 5 and 10 khz

with instantaneous peaks at 18 khz for $t = \{0, T/4, T/2, 3T/4\}$. This average switching frequency was found as predict mainly dependent on the boost dimensioning and the load. To conclude the presentation of this work, we present in Fig. 12 showing the clear form of the output of the symmetrical boost-discharge converter under proteus.
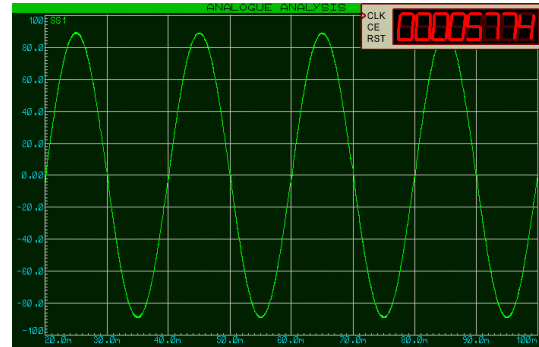

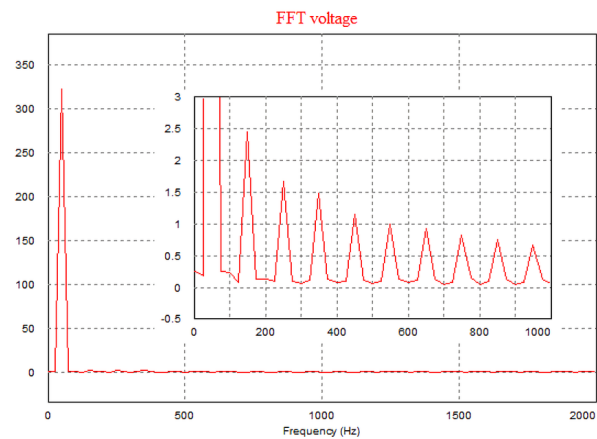**Fig. 12:** Voltage Invertir (Proteus).

Fig. 13: FFT analysis of the output transformer voltage.

Fig. 13 depicts the FFT analysis of the output voltage from the transformer. The maximum amplitude of the fundamental voltage reaches 321 V. Furthermore, it is evident from Fig. 13 that the harmonic voltages generated by the inverter are odd multiples of the fundamental frequency, which is 50 Hz. The third harmonic stands out, displaying a maximum amplitude of 2.5 V. In a general context, the amplitude of each harmonic voltage diminishes proportionally with its frequency.

4. Conclusion

The symmetrical boost-discharge converter developed in this study and discussed in this paper is based on an original topology integrating a minimum of components ensuring the conversion in two stages in cascade. We have shown that this topology associated with an original control allows a conversion of DC/AC voltages

coming from a renewable energy source and feeding a 220 V AC load, with an interesting total harmonic distortion rate lower than 2% and a good conversion efficiency estimated at 92%, as well as a a good robustness to load variations. However, power switches must withstand a switching frequency ranging from a few 2 kHz to 20 kHz. These two values represent the lower and upper limits between which the frequency varies over a single half-period; these limits are directly imposed by the control. The average switching frequency value ranges from 5 kHz to 10 kHz.

The simulations also highlight some improvements to be made, such as reducing the average switching frequency. the control used, although very powerful, creates a permanent error. As a result, the voltage is slightly higher than the reference and does not allow a perfect zero crossing. These problems must be minimized in order to improve this topology.

Author Contributions

GHRIBI proposed the idea, carried out the modeling, demonstrated stability, and performed simulations. TERNIFI, BACHIR, and AILLERIE validated the simulations, mathematical model, and stability. All authors discussed the results and contributed to the final manuscript writing.

References

[1] DAS, M. K., S. MISHRA, and K. C. JANA. Novel 21-level Reduced Switches Inverter. *IEEE International Conference on Power Electronics, Drives and Energy Systems (PEDES)*. 2022, pp. 1-6. ISBN 978-1-6654-5566-4. DOI: 10.1109/PEDES56012.2022.10080285.

[2] SHAH, M. J., K. S. PANDYA, and CHAUHAN. An MPPT-based 31-Level ADC Controlled Micro-Inverter. *Technology Applied Science Research.* 2022, vol. 12, iss. 5, pp. 1200-1205. ISSN 1792-8036. DOI: 10.48084/etasr.5199.

[3] MONDAL, S., S. P. BISWAS , M. R. ISLAM and S. M. MUYEEN . A Five-Level Switched-Capacitor Based Transformerless Inverter With Boosting Capability for Grid-Tied PV Applications. *IEEE Access* 2023, vol. 11, pp. 12426–12443. ISSN: 2169-3536. DOI: 10.1109/ACCESS.2023.3241927

[4] MAAMAR, A. E. T. Analysis and Experimental Validation of Selective Harmonic Elimination in Single-Phase Five-Level Inverter using Particle Swarm Optimization Algorithm. *Electronics*

2022, vol. 26, iss. 2 , pp. 65–72. ISSN:1450-5843. DOI: 10.53314/ELS2226065M

[5] LAHOOTI ESHKEVARI, A., A. MOSALLANE-JAD, M. S. SEPASIAN . A new configuration for four-switch three-phase inverters based on a switched-capacitor step-up cell for electric vehicles application. *Turkish Journal of Electrical Engineering and Computer Sciences* 2020; vol. 28, iss. 6, Article 21. ISSN:1303-6203 . DOI: 10.3906/ELK-2005-141

[6] KARIMI, E., B. M. TEHRANI and E. ADIB .A Soft-Switching Double-Input Micro-Inverter. *IEEE Transactions on Industrial Electronics* 2021; vol. 68, iss .8, pp. 6721–6728. ISSN:1557-9948. DOI: 10.1109/TIE.2020.3000124

[7] JAIN, S. and V. AGARWAL. A single-stage grid connected inverter topology for solar PV systems with maximum powerpoint tracking. *IEEE Trans. Power Electron* 2007, vol. 22, iss.5, pp. 1928-1940, ISSN: 0885-8993. DOI: 10.1109/TPEL.2007.904202

[8] GARCÍA-RODRÍGUEZ, V. H., J. H. PÉREZ-CRUZ, R. C. AMBROSIO-LÁZARO and S. TAVERA-MOSQUEDA. Analysis of DC/DC Boost Converter– Full-Bridge Buck Inverter System for AC Generation. *Energies 2023*, vol. 16, iss. 6, 2509. ISSN: 1996-1073. DOI: 10.3390/en16062509

[9] HUYNH, A. T., A. V. HO and T. W. CHUN. Switched-Capacitor-Inductor Active-Switched Boost Inverters with High Boost Ability. *IEEE Access* 2021, vol. 9, pp. 101543–101554. ISSN: 2169-3536. DOI: 10.1109/ACCESS.2021.3097371

[10] RAHMOUNI, W., G. BACHIR and M. AILLERIE. A new control strategy for harmonic reduction in photovoltaic inverters inspired by the autonomous nervous system. *Journal of Electrical Engineering* 2022, vol. 7, iss. 5, pp. 310–317. ISSN:1339-309X DOI: 10.2478/jee-2022-0041

[11] TERNIFI, Z. E. T., G. BACHIR and M. AILLERIE. A single-phase photovoltaic microinverter topology based on boost converter. *Przeglad Elektrotechniczny* 2019; vol. 95, iss. 4, pp. 215–217. ISSN: 2449-9544. DOI: 10.15199/48.2019.04.40

[12] CHANG, C. H. and Y, F CHEN . A transformerless buck-boost grid-tied inverter with low leakage-current and high voltage-gain. *Appl.Sci.* 2021, vol. 11, iss. 8, 3625. ISSN: 2076-3417. DOI: 10.3390/app11083625

[13] SÉGUIER, G., P. DELARUE and F. LABRIQUE. Électronique de puissance, Structures, commandes, applications. DUNOD, 10E ÉDITION 2015, ISBN: 2100739751.

[14] TAYLOR and FRANCIS. Lyapunov AM. The General Problem of the Stability of Motion. London, UK: LTD., 1992 , ISBN: 0748400621.

[15] ATES, M. and S. LARIBI. New results on the global asymptotic stability of certain nonlinear RLC circuits, *Turkish Journal of Electrical Engineering and Computer Sciences.* 2018, vol. 26, iss. 1 , Article 36. ISSN: 1300-0632. DOI: 10.3906/elk-1612-100

[16] DONG, C. S. T. , H. H. VO ,T. C. TRAN, P. BRANDSTETTER and P. SIMONIK. Application of sensorless sliding mode observer in control of induction motor drive. *Advances in Electrical and Electronic Engineering.* 2017, vol. 15,iss. 5, pp. 747–753. ISSN: 1336-1376. DOI: 10.15598/aeee.v15i5.2626

About Authors

Mohammed El Bachir GHRIBI was born in Oran (Algeria) in 1999. He is currently a PhD student at the University of Science and Technology of Oran, Algeria, where he is a member of the Laboratory of Applied Power Electronics (LEPA). His main research interests are power systems, power electronics and renewable energies

Zine Eddine Touhami TERNIFI is a researcher in Electrotechnique at the University of Science and Technology of Oran (USTO), with a PhD in Electrical Engineering focused on Photovoltaic Systems (2019). Touhami's research focuses on the development of and improvements to static converters that are dedicated to photovoltaic systems, in order to improve their control and efficiency as generators of electricity. As part of his research endeavors, Touhami actively mentors and supervises photovoltaic project work for final-year students at USTO. He also serves as a lecturer at the University of Science and Technology of Oran, within the Faculty of Electrical Engineering, Department of Electrotechnique, teaching modules directly related to the field of photovoltaics. He has published articles on photovoltaic microinverter topologies and has presented his research at international conferences. His expertise includes programming, simulation of electrical circuits, and technological research. With a diverse skill set and multilingual proficiency, Touhami is poised to make notable contributions to the renewable energy sector.

Ghalem BACHIR was born in Oran in Algeria. He is currently a professor at the University of Science and technology of Oran with a degree of professor of the universities. He is a team leader in the 'LDDEE' research laboratory whose main theme is research in renewable energies.

Michel AILLERIE obtained a PhD in 1991 and the Habil-tation to Lead Researches in 2001 at the Universite Paul Verlaine of Metz, currently Universite de Lorraine. He is Professor since 2005 and makes his research in the city of Metz at the Laboratoire Materiaux Optiques et Photonique, LMOPS, join laboratory of the Universite de Lorraine and Centrale-Supelec Universite de Paris-Saclay, France. He is researcher in the team "Materials, Components and Systems for Photovoltaic" for which he is the leader. His interests and activities concern two main themes. The first one concerns the Characterization of functional non-linear optical properties of materials for optoelectronic applications. The second one concerns the development and optimization of energy production and management systems in a sustainable development approach.